Overlapping Control Volume Method for Solute Transport

By Atul Kumar Verma,[1] S. Murty Bhallamudi,[2] and V. Eswaran[3]

ABSTRACT: In this paper, an overlapping control volume method is presented for the numerical solution of transient 2D solute transport problems in ground water. The method is applicable for nonorthogonal grids and uses an isoparametric formulation for computing the dispersion and for second-order upwinding. Time integration is performed using an implicit approach. Three test cases are considered for comparing the numerical with analytical solutions. The scheme is second order in space and, when combined with Crank-Nicholson, is also second order in time. The results using Crank-Nicholson and full implicit (first-order) time integration methods are compared for problems with a variety of boundary conditions. For diffusion-dominated flows ($P_\Delta \leq 2$) Crank-Nicholson works well, but for convection-dominated flows it produces spurious oscillations due to numerical dispersion errors. These oscillations are controlled by a flux limiter but only for Courant numbers below unity. It is shown that for high Courant and Péclet numbers a slight weighting of the time stepping toward fully implicit is effective against spurious oscillations and offers an optimum compromise between numerical dissipation and dispersion errors for a wide range of Courant and Péclet numbers. The scheme is shown to work on mildly nonorthogonal grids.

INTRODUCTION

Modeling the transport of dissolved solutes in ground-water flows of practical interest requires the numerical solution of a transient convection-dispersion equation in two or more dimensions. The numerical schemes for these equations need to have sufficient accuracy and also be adaptable to complex geometries, which are common in practical applications of solute-transport problems. The accuracy of a scheme is classified by its order of accuracy in space and time. Integrations of first-order accuracy have diffusive errors, which tend to spread the solution at sharp fronts. Therefore, second-order integration schemes are preferable for problems with such fronts. However, second-order schemes tend to produce solutions with spurious oscillations at the fronts. In recent years there has been much activity in the development of flux limiters, which suppress these oscillations (Hirsch 1991).

Finite-element methods (FEMs) are popular for solving the transport equations [e.g., Huyakorn and Pinder (1983)]. Finite-difference methods, although simple and easy to apply in rectangular domains, have difficulty in handling complex geometries. The FEMs are algorithmically more complex but can be applied on irregular geometries. One of the main problems with the conventional Galerkin finite-element formulation is its inability to handle convection-dominated flows. Van Genuchten (1977), Pinder and Shapiro (1979), Heinrich et al. (1977), Sun and Yeh (1993), Wang et al. (1986), Yeh (1986), and Westerink and Shea (1986) have developed FEMs that attempt to minimize the numerical oscillations in various ways. Yu and Singh (1996) developed a modified Galerkin FEM for solute transport.

Eulerian-Lagrangian methods have also been developed in recent years for the solution of transport equations. In these methods, the advection-dispersion equation is decomposed into two parts, one modeling pure advection and the other dispersion. The Lagrangian approach is used for the advection part and the Eulerian approach for the dispersion part. These techniques reduce the numerical oscillations but produce false diffusion at the front. Yeh (1990), Yeh and Chang (1992), and Ijiri and Karasaki (1994) used various techniques to minimize this diffusion. These schemes achieve a better accuracy at the expense of higher computational costs, especially when 2D transport is involved.

Finite-volume techniques offer a viable alternative to FEMs for solving flow and transport problems (Peyret and Taylor 1983). They combine the flexibility of handling complex geometries, intrinsic to FEM, with the simplicity of finite-difference methods. Putti et al. (1990) developed a triangular finite-volume technique for solving the ground-water solute transport equation. This method uses a monotone interpolation scheme to avoid the numerical oscillations at sharp concentration fronts in advection-dominated flows. This is an explicit method in which the computational time step is restricted by considerations of numerical stability. This often increases the computational burden, especially in long-period simulations that are common in solute transport problems. Cox and Nishikawa (1991) presented a total variation diminishing scheme based on rectangular orthogonal elements. This method is also based on an explicit formulation for the time stepping.

Recently, Verma and Eswaran (1996) introduced an overlapping control volume (OCV) technique for solving the steady convection-diffusion equation in arbitrary 2D domains on nonorthogonal grids. They use an isoparametric formulation to compute diffusion and to introduce a higher order upwinding. The scheme is in many ways comparable to the QUICK scheme (Leonard 1979). The scheme was shown to have second-order accuracy in space and to be computationally efficient. The method can be used on nonorthogonal geometries and with Dirichlet, Neumann, and Robin boundary conditions. Flux limiting has also been applied to the OCV formulation by Verma and Eswaran (1997), who extended the previous work to the explicitly (first-order) time-integrated transient case and incorporated a flux limiter into the scheme.

In this paper, the OCV technique is extended to address the specific problem of multidimensional transient solute transport in ground water. However, the algorithm can also be used in computational fluid dynamics and other areas. The formulation in this paper has the following unique features, beyond the limits of the above two cited papers:

- It can handle a variable tensorial diffusivity, which is common in solute transport.
- The time stepping is implicit and unconditionally stable (solute transport problems often have long integration times, which are expensive for explicit schemes restricted by a conditional stability criterion).

[1]Formerly, Grad. Student, Dept. of Mech. Engrg., Indian Inst. of Technol., Kanpur 208016, India.

[2]Dept. of Civ. Engrg., Indian Inst. of Technol., Madras 600036, India.

[3]Dept. of Mech. Engrg., Indian Inst. of Technol., Kanpur 208016, India.

- The scheme, already second-order accurate in space, is combined with the Crank-Nicholson time-stepping scheme to be second-order in time as well.
- Satisfactory results can be obtained for a large range of grid Péclet numbers (to at least 2,000) and Courant numbers (to 4), which makes it suitable for large time-step integrations of both diffusions and convection-dominated flows.

This paper presents the formulation of the scheme and the results of three test cases that demonstrate its capabilities. The issue of suppression of spurious oscillations is also addressed. It is shown that a judicious choice of the implicit weighting factor with a previously developed flux limiter (Verma and Eswaran 1997) is highly efficient in suppressing oscillations.

GOVERNING EQUATIONS

The governing equation for solute transport under saturated ground-water flow conditions is given by (Freeze and Cherry 1979)

$$R_d \frac{\partial C}{\partial t} = \nabla \cdot (\mathbf{D}_h \cdot \nabla C) - \nabla \cdot (\mathbf{V} C) - \lambda R_d C \qquad (1)$$

where C = solute concentration; $\mathbf{V}$ = pore-water velocity vector; R_d = retardation factor; λ = first-order decay coefficient; $\mathbf{D}_h$ = hydrodynamic dispersion tensor; and t = time. The elements of the dispersion tensor D_{xx}, D_{zz}, D_{xz} ($=D_{zx}$) are generally functions of velocity and the molecular diffusion. In the present study, the case of a homogeneous and isotropic medium under 2D ground-water flow with 2D dispersion is considered. However, the numerical scheme is a general one and can be applied to nonhomogeneous, nonisotropic conditions.

FINITE-VOLUME FORMULATION

The solution domain is discretized into a structured non-orthogonal grid as shown in Fig. 1(a) and a control volume as shown in Fig. 1(b) is considered. The choice of control volume does not involve the determination of any intermediate points and uses the grid point coordinates directly to form the control volumes. Each control volume is labeled by the index of the central node [e.g., the control volume for (i, j) is shown in Fig. 1(b)]. It can be seen that adjacent control volumes will overlap each other, hence the name "overlapping control volume" technique.

On integrating (1) over the control volume and applying the Gauss-divergence theorem, we get

$$\iint R_d \frac{\partial C}{\partial t} \, dA = \oint_{cs} \left[\left(D_{xx} \frac{\partial C}{\partial x} + D_{xz} \frac{\partial C}{\partial z} \right) n_x \right] dl$$

$$+ \oint_{cs} \left[\left(D_{zx} \frac{\partial C}{\partial x} + D_{zz} \frac{\partial C}{\partial z} \right) n_z \right] dl$$

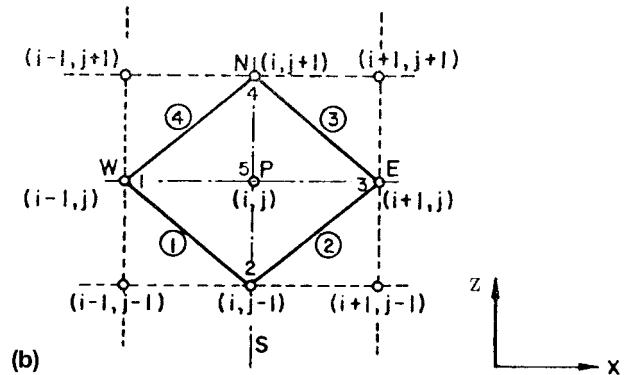$$- \int_{cs} C(u n_x + w n_z) \, dl - \iint \lambda R_d C \, dA \qquad (2)$$

where dl = elemental length on the boundary (control surface) of the control volume; n_x and n_z = direction cosines of the local outward unit vector on the boundary in x and z directions, respectively; and dA = elemental area of the control volume. Eq. (2) can be partially discretized as

$$\frac{R_d A_s}{\Delta t} (C^{n+1} - C^n) = \theta[DIFF]^{n+1} + (1 - \theta)[DIFF]^n + \theta[CONV]^{n+1}$$

$$+ (1 - \theta)[CONV]^n + \theta[DEC]^{n+1} + (1 - \theta)[DEC]^n \qquad (3)$$
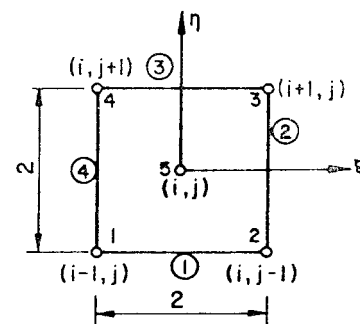
where
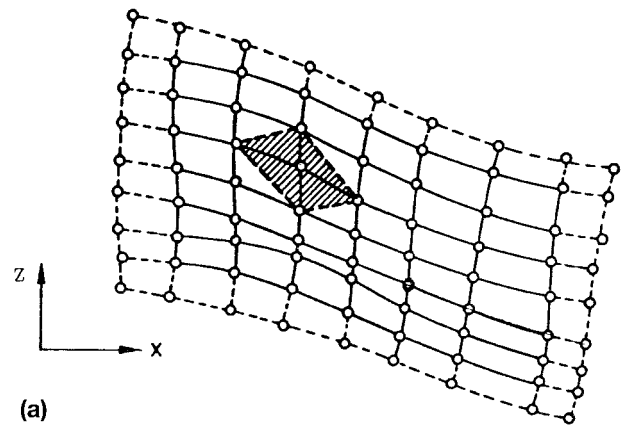
(a)

(b)

(c)

FIG. 1. Definition Sketch for Control Volume Formulation

$$DIFF = \oint_{cs} \left[\left(D_{xx} \frac{\partial C}{\partial x} + D_{xz} \frac{\partial C}{\partial z} \right) n_x + \left(D_{zx} \frac{\partial C}{\partial x} + D_{zz} \frac{\partial C}{\partial z} \right) n_z \right] dl$$

$$CONV = -\oint_{cs} C(u n_x + w n_z) \, dl$$

$$DEC = -\lambda R_d C A_s$$

A_s = area of the control volume; Δt = computational time step; and θ = weight parameter, which is equal to 0.0 for explicit schemes and 1.0 for fully implicit schemes. If θ is equal to 0.5 we get the Crank-Nicholson scheme, which is second-order time accurate. Superscripts n and $n + 1$ in (3) denote the evaluation of the terms at the time levels t and $t + \Delta t$, respectively.

The contour integration for the terms on the right-hand side of (3) is counterclockwise. These terms are further discretized as described in the following sections.

Convection Term

The midpoint rule is used to approximate the convective term

$$\oint_{cs} C(un_x + wn_z)\, dl = \sum_{k=1}^{4} C^{(k)}(u^{(k)}\Delta z^{(k)} - w^{(k)}\Delta x^{(k)}) = \sum_{k=1}^{4} C^{(k)}F^{(k)} \tag{4}$$

where the superscript (k) refers to the edges of the control volume [see Fig. 1(b)]; and $F(k)$ is the fluid flux across edge k. The quantities $\Delta x^{(k)}$ and $\Delta z^{(k)}$ are the changes in the coordinates along the edge, i.e., $\Delta x^{(k)} = x_{m+1} - x_m$ and $\Delta z^{(k)} = z_{m+1} - z_m$ (note these can be negative), where the subscript m refers to the node number. The velocity components $u^{(k)}$ and $w^{(k)}$ are the averages of the values at the end points of the edge k.

The outward volume rate of flow through the edge k, $F^{(k)}$ is given by

$$F^{(k)} = (u^{(k)}\Delta z^{(k)} - w^{(k)}\Delta x^{(k)}) \tag{5}$$

To incorporate the second-order upwinding, $C^{(k)}$ in (4) is approximated at the midpoint of control surface k by interpolation within the upwind control volume adjacent to the surface. For example, referring to Fig. 1(b), if the flow is leaving the control volume (i, j) across face 1 (i.e., $F^{(1)}$ is positive), then $C^{(1)}$ is approximated by interpolation within the control volume for node (i, j). The values at the grid points constituting the control volume (i, j) are used for determining $C^{(1)}$. On the other hand, if $F^{(1)}$ is negative, the values at the grid points of the control volume ($i - 1, j - 1$) are used to obtain $C^{(1)}$. The interpolation scheme to obtain the $C(k)$ value at face k is based on mapping of the cell (Verma and Eswaran 1996) onto a 2×2 square in a $\xi - \eta$ space [Fig. 1(c)]. The interpolation is then done using finite-element type shape functions

$$N_1 = 0.25(-\xi - \eta + \xi\eta) + 0.125(\xi^2 + \eta^2) \tag{6a}$$

$$N_2 = 0.25(\xi - \eta - \xi\eta) + 0.125(\xi^2 + \eta^2) \tag{6b}$$

$$N_3 = 0.25(\xi + \eta + \xi\eta) + 0.125(\xi^2 + \eta^2) \tag{6c}$$

$$N_4 = 0.25(-\xi + \eta - \xi\eta) + 0.125(\xi^2 + \eta^2) \tag{6d}$$

$$N_5 = 1 - 0.5(\xi^2 + \eta^2) \tag{6e}$$

which are used for the isoparametric interpolation of

$$x = \sum_{i=1}^{5} N_i x_i \tag{7}$$

$$z = \sum_{i=1}^{5} N_i z_i \tag{8}$$

$$C = \sum_{i=1}^{5} N_i C_i \tag{9}$$

where the subscript i refers to the node number [see Fig. 1(b)]. The value of $C^{(k)}$ is determined, for upwinding, at the midpoint (in ξ, η space) of any edge k by first determining $N_1, N_2, N_3, \ldots, N_5$ for the corresponding ξ and η values (e.g., $\xi = 0$ and $\eta = -1$ for $k = 1$) of the upwind cell and then using (9).

Diffusion Term

The diffusion term is also approximated using the midpoint rule. This term is discretized as given below

$$\oint_{cs} \left[\left(D_{xx}\frac{\partial C}{\partial x} + D_{xz}\frac{\partial C}{\partial z} \right) n_x + \left(D_{zx}\frac{\partial C}{\partial x} + D_{zz}\frac{\partial C}{\partial z} \right) n_z \right] dl$$

$$= \sum_{k=1}^{4} \left[D_{xx}^{(k)}\left(\frac{\partial C}{\partial x}\right)^{(k)} + D_{xz}^{(k)}\left(\frac{\partial C}{\partial z}\right)^{(k)} \right] (\Delta z)^{(k)}$$

$$- \sum_{k=1}^{4} \left[D_{zx}^{(k)}\left(\frac{\partial C}{\partial x}\right)^{(k)} + D_{zz}^{(k)}\left(\frac{\partial C}{\partial z}\right)^{(k)} \right] (\Delta x)^{(k)} \tag{10}$$

where $D_{xx}^{(k)}$, $D_{zz}^{(k)}$, and $D_{xz}^{(k)}$ are again determined using averages of the end-point values and $(\partial C/\partial x)^{(k)}$ and $(\partial C/\partial z)^{(k)}$ are determined at the midpoint (again in ξ, η space) of the edge k using the derivatives of the shape functions N_i

$$\left(\frac{\partial C}{\partial x}\right)^{(k)} = \sum_{i=1}^{5} \left(\frac{\partial N_i}{\partial x}\right)^{(k)} C_i \tag{11}$$

$$\left(\frac{\partial C}{\partial z}\right)^{(k)} = \sum_{i=1}^{5} \left(\frac{\partial N_i}{\partial z}\right)^{(k)} C_i \tag{12}$$

where the derivatives of the shape functions are computed during the initialization procedure and stored for subsequent use.

Decay Term

The decay term DEC in (3) is computed using the scalar value C at the cell center.

Boundary Conditions

In the earlier study (Verma and Eswaran 1996), boundary conditions were implemented through the use of additional fictitious points along the domain boundary. These additional points were needed for the upwinding and diffusion term calculations at the grid points on the boundary. The values of scalar C at these fictitious points were specified using a quadratic extrapolation. In this study, simple (i.e., first-order) upwinding is used for cell faces next to the boundary. This allows for a direct implementation of both Dirichlet and Neumann boundary conditions. Numerical experimentation has indicated that the difference in results obtained using the above two methods is not significant for the problems studied here.

Solution Procedure

Finally, with the above formulation, the discretized equation for (1) can be written

$$a_p C_p = \sum_{nb} a_{nb} C_{nb} + b \tag{13}$$

where C_p = (unknown) concentration value at the central node; C_{nb} = (unknown) values at the neighbors (including those for neighboring control volumes introduced by upwinding); and b = sum of known quantities. The coefficients a_p and a_{nb} are given in Appendix I. The Gauss-Seidel iterative technique is used to solve the discretized equation. The coefficient matrix may lose its diagonal dominance in highly convective flows and the iterative scheme thus may become unstable. To facilitate iterative convergence, the terms with negative coefficients in the summation in (13) are approximated by previous iteration values and transferred to b. This improves the numerical convergence properties of the algorithm without affecting its discretization consistency, because the converged solution satisfies the original discrete equations. No difficulties were encountered in solving the variety of test problems using this procedure.

FLUX LIMITER

There has been considerable interest in recent years on the use of total variation diminishing and flux-limiting schemes to avoid the overshoots/undershoots inherent in second-order solutions of flows with sharp gradients [e.g., Hirsch (1991)]. Mostly, flux-limiting schemes have been used with steady-state formulations or explicit time-integration schemes. A flux-limiting scheme has been developed for the OCV method. The flux limiter has shown itself to be effective in removing oscillations in steady-state and explicitly time-stepped problems (Verma and Eswaran 1997).

The algorithm developed by Verma and Eswaran (1997)

uses second-order upwinding normally but switches to first-order upwinding in abnormal cells where second-order upwinding would cause unboundedness. A cell is considered to be abnormal when the scalar value at the central node is outside the range of values at the cell corners. The algorithm is given in detail in the referred paper and hence is not repeated here. The above flux limiter is used here without any major modifications, the only difference being the use of "estimated" values in the implicit iterations instead of the known values as in the explicit solution.

RESULTS

Three test cases of transient 2D transport in porous media are considered in this section. In the first two cases, we compute the transport of a scalar in rectangular domains with three different types of boundary conditions. The solution with Crank-Nicholson and fully implicit time-stepping schemes are compared. The third case considers nonrectangular domains and nonorthogonal grids; methods are presented for the suppression of spurious oscillations in the solutions, and the scheme's applicability for a wide range of Courant and grid Péclet numbers is demonstrated. In all cases, comparisons are done with known analytical solutions. The accuracy of different time-stepping schemes for the OCV method is investigated and the circumstances under which spurious oscillations arise and methods for their removal are discussed.

Test Problem 1: Dirichlet Boundary Condition at Source

Test Problem 1 considers unsteady 2D solute transport between two impervious boundaries. A finite-length strip solute source, whose concentration is a given function of time, is located asymmetrically along the z-axis at $x = 0$ in a unidirectional seepage velocity field, as shown in Fig. 2. The rectangular domain is 75 m in the x-direction and 50 m in the z-direction. The geometrical parameters for the source (Fig. 2) are $B_1 = 5$ m, $B_2 = 10$ m, and $B_3 = 35$ m. The uniform pore velocity u is 0.1 m/day. The longitudinal, transverse, and cross dispersivities, D_{xx}, D_{zz}, and D_{xz}, are 1.0, 0.1, and 0.0 m²/day, respectively. The retardation factor R_d is 1.0, and the decay coefficient λ is 0.0. The initial condition is given by $C(x, z, 0) = 0$. The boundary condition at $x = 0$, $t > 0$, is given by

$$C(0, z, t) = 0, \quad 0 < z < B_1 \tag{14a}$$

$$C(0, z, t) = 1.0, \quad B_1 < z < B_1 + B_2 \tag{14b}$$

$$C(0, z, t) = 0, \quad B_1 + B_2 < z < z_m \tag{14c}$$

The analytical solution for the above problem is given by Batu (1989). The computational domain is represented by 61 × 41 (in the x- and z-directions, respectively) grid points, and the computational time step Δt is 1 day. The Courant number ($\equiv u\Delta t/\Delta x$) is $C_n = 0.08$, and the longitudinal grid Péclet number ($\equiv u\Delta x/D_{xx}$) is $P_\Delta = 0.125$. Here, and in the next test problem, the same grids and numerical parameters are used as were used by Batu (1989, 1993) in the numerical validation of the analytical solutions. Fig. 3 presents the longitudinal concentration distributions at $t = 100$ days as a function of x for $z = 10$ and 16.25 m. Fig. 4 presents the lateral concentration distributions for $x = 5$ and 20 m. The numerical results in these figures are obtained using the Crank-Nicholson scheme ($\theta = 0.5$) and the fully implicit scheme ($\theta = 1.0$). As can be seen from these figures, the method gives accurate solutions. To examine numerical stability for Courant numbers greater than unity, computations are made with 121 × 81 grid points and $\Delta t = 10$ days ($C_n = 1.6$). The computed results for this case obtained using the implicit scheme are compared with the analytical results in Fig. 5. Although stable results could be ob-
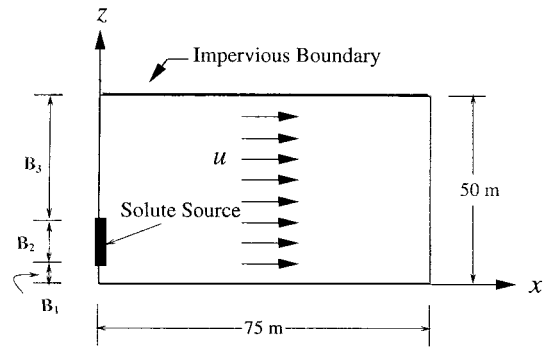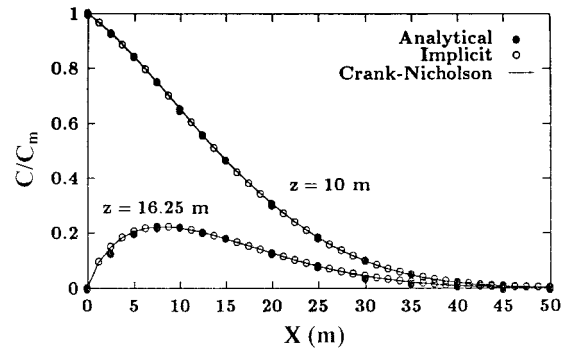

FIG. 2. Schematic of Test Problem 1

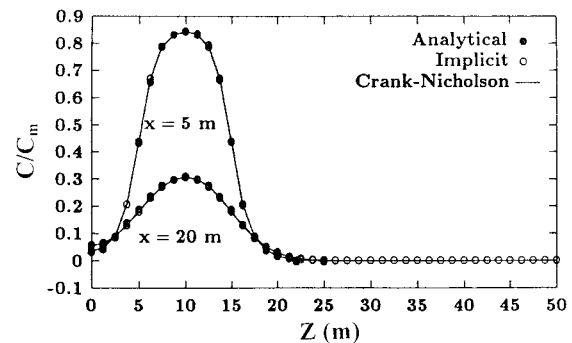FIG. 3. Longitudinal Concentration Profile: Test Problem 1 (Grid = 61 × 41, $\Delta t = 1$ Day)

FIG. 4. Transverse Concentration Profile: Test Problem 1 (Grid = 61 × 41, $\Delta t = 1$ Day)
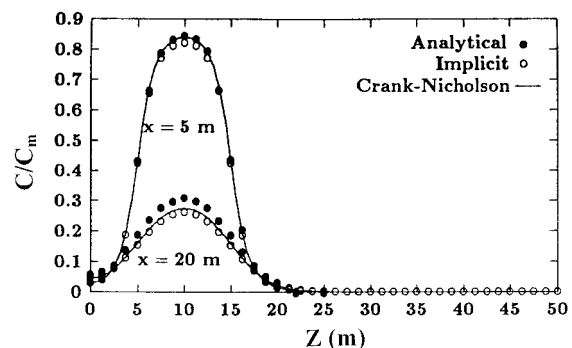

FIG. 5. Transverse Concentration Profile: Test Problem 1 (Grid = 121 × 81, $\Delta t = 10$ Days)

tained using the OCV scheme, there is somewhat more error in the numerical solution. This is expected because the most accurate results are generally obtained when $C_n = 1$. The fully implicit scheme, which is only first-order accurate in time, introduces noticeably larger errors than the Crank-Nicholson scheme.

Test Problem 2: Mixed Boundary Condition at Source

This example considers the 2D solute transport in a unidirectional flow field with mixed (Robin) type boundary conditions at the source. A finite-length strip solute source is located asymmetrically along the z-axis at $x = 0$ in a unidirectional velocity field, as shown in Fig. 6. The domain is 185 m in the x-direction and 53 m in the z-direction. The geometrical parameters for the source (Fig. 6) are $B_1 = 45$ m, $B_2 = 5$ m, and $B_3 = 3$ m. The uniform pore velocity u is equal to 0.15 m/day. The longitudinal, transverse, and cross dispersion coefficients, D_{xx}, D_{zz}, and D_{xz}, are equal to 3.195, 0.645, and 0.0 m^2/day, respectively. The retardation factor and the decay coefficient are equal to 1.0 and 0.0, respectively. The initial condition is given by $C(x, z, 0) = 0$. Boundary condition is given by

$$F_x(0, z, t) = 0, \quad 0 < z < B_1 \tag{15a}$$

$$F_x(0, z, t) = uC_m, \quad B_1 < z < B_1 + B_2 \tag{15b}$$

$$F_x(0, z, t) = 0, \quad B_1 + B_2 < z < z_m \tag{15c}$$

where $C_m = 1.0$; and F_x = convective-dispersive flux component (the mass flow rate of solute per unit area) in the x-direction

$$F_x = \Phi u C - \Phi D_{xx} \frac{\partial C}{\partial x}$$

$$F_z = -\Phi D_{zz} \frac{\partial C}{\partial z}$$

where Φ = porosity (=0.25 for the problem under consideration).

The analytical solution for the above problem is given by Batu (1993). In the numerical solution, the computational domain is divided into 48×29 nonuniform grid points (closer mesh spacing near the upstream boundary), and Δt is equal to 1 day ($C_n = 0.04$, $P_\Delta = 0.18$). The numerical results for the
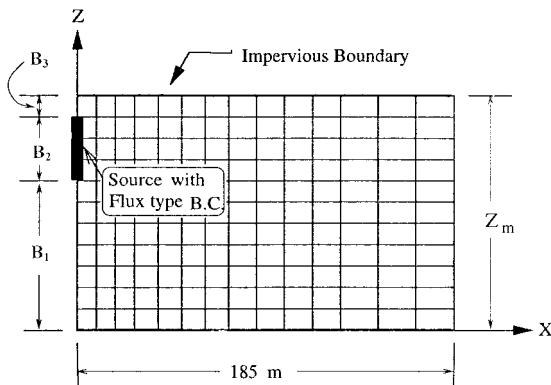
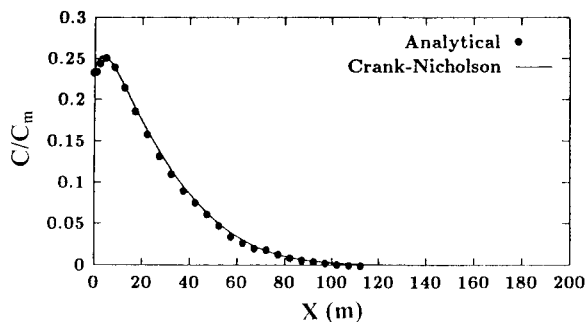**FIG. 6. Schematic of Test Problem 2**

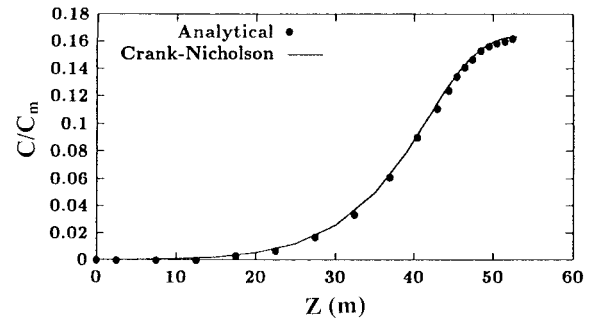**FIG. 7. Longitudinal Concentration Profile at $z = 51.5$ m: Test Problem 2**

FIG. 8. Transverse Concentration Profile at $x = 22.5$ m: Test Problem 2
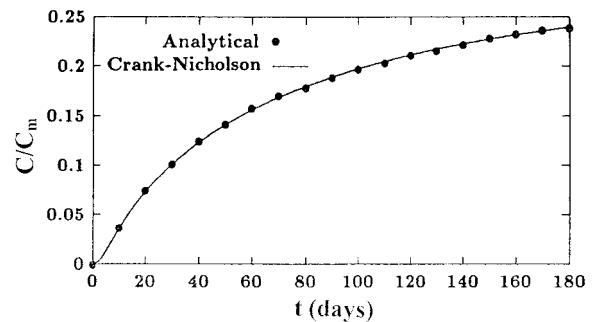
FIG. 9. Temporal Variation at x, $z = 8.75$, 47.5 m: Test Problem 2

normalized concentration obtained using the Crank-Nicholson scheme ($\theta = 0.5$) are compared with the analytical solution in Figs. 7–9. Longitudinal and transverse concentration versus distance comparison at $x = 51.5$ and 22.5 m are shown in Figs. 7 and 8, respectively, at a 180-day period. Fig. 9 presents the time variation of the normalized concentration at the point x, $z = 8.75$, 47.5 m. As can be seen from these figures, a good correspondence exists between the numerical results and the analytical results.

Test Problem 3: Nonrectangular Domain

In this example, a nonrectangular domain with a nonorthogonal grid, as shown in Fig. 10, is considered. The length of the domain along the x-axis L is 10 m; its lateral boundaries are given by the equation

$$z = \pm \left[2.0 + 1.05 \sin\left(\frac{\pi x}{2L}\right) \right] \tag{16}$$

A strip source of length 1 m is placed center-symmetrically along the z-axis at $x = 0$ in a uniform velocity field. The retardation factor and the decay coefficients are equal to 1.0 and 0.0, respectively, and $u = 0.2$ m/day. The initial condition is given by $C(x, z, 0) = 0$. The boundary condition at $x = 0$ is given by

$$C(0, z, t) = 1, \quad \text{at the source} \tag{17a}$$

$$C(0, z, t) = 0, \quad \text{elsewhere} \tag{17b}$$

Dirichlet boundary conditions are applied at the lateral boundaries. For the specification of the time varying concentrations along the lateral boundaries, the analytical solution given by Javendel et al. (1984) for the semi-infinite domain is used. The analytical solution can be written

$$C(x, z, t) = \frac{x}{4\sqrt{(\pi D_{xx})}} \exp\left(\frac{ux}{2D_{xx}}\right) \int_0^t \exp\left[-\frac{u^2 t}{4D_{xx}} - \frac{x^2}{4D_{zz}t} \right] \frac{1}{t^{3/2}}$$

$$\cdot \left[\text{erf}\left(\frac{a-z}{2\sqrt{(D_{zz}t)}}\right) + \text{erf}\left(\frac{a+z}{2\sqrt{(D_{zz}t)}}\right) \right] dt$$

FIG. 10. Grid Layout for Test Problem 3
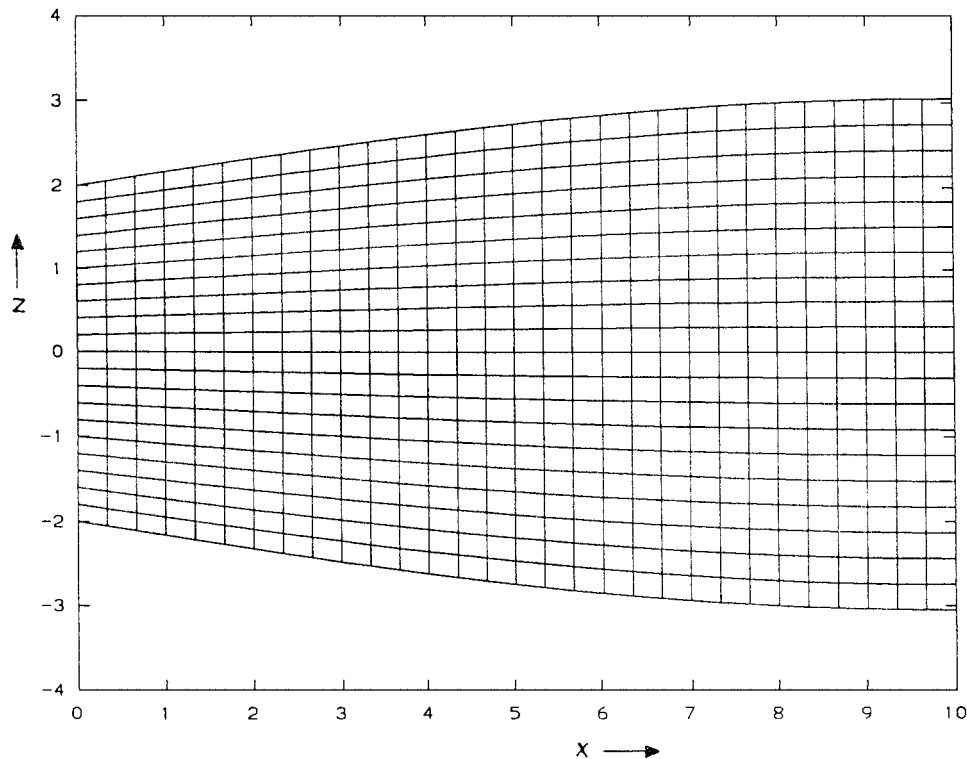

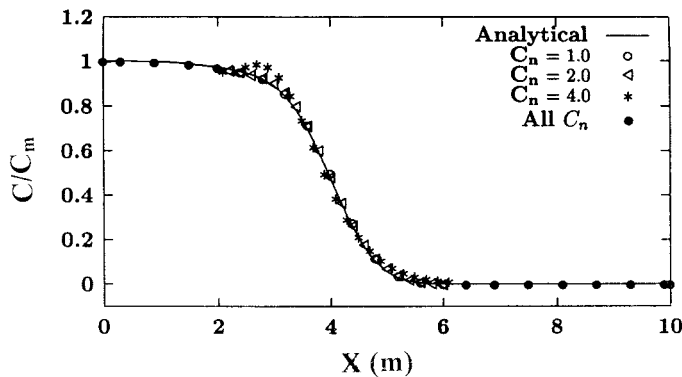**FIG. 11. Longitudinal Concentration Profile: Test Problem 3 ($P_\Delta = 2$)**

FIG. 12. Longitudinal Concentration Profile: Test Problem 3 ($P_\Delta = 40$)

where a = half-width of the strip source at $x = 0$. A fourth-order numerical integration is used to evaluate the above equation to obtain the concentration at the lateral boundaries, to supply the boundary conditions, as well as at any interior point if needed for comparison with the numerical solution. The computational domain is divided into 100×81 grid points. The time step Δt is taken as 0.1, 0.5, 1.0, and 2.0 days, and the corresponding Courant number C_n is 0.2, 1.0, 2.0, and 4.0, respectively.

In the previous sections the Crank-Nicholson scheme has been shown to be more accurate than fully implicit time stepping. Therefore, we first investigate the solutions obtained using the Crank-Nicholson scheme for this problem. Fig. 11 shows the Crank-Nicholson solution, for various Courant numbers, for the problem at $t = 20$ days; the longitudinal grid Péclet number P_Δ is a moderate value of 2.0 ($D_{xx} = 0.01$ m²/day, $D_{zz} = 0.0025$ m²/day). The solutions for Courant numbers of 1.0 and 2.0 are good, whereas the solutions for $C_n = 4.0$ are acceptable, showing only a slight overshoot. The solutions for C_n below unity all fall on the analytical solution but are not shown (to avoid clutter).

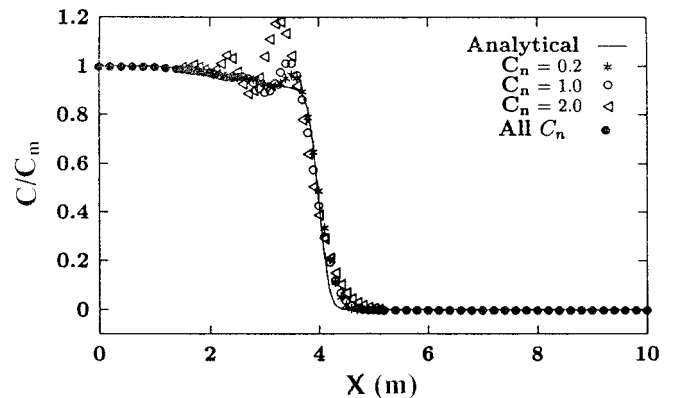Fig. 12 shows for the same situations the Crank-Nicholson

solutions for a grid Péclet number of 40.0 ($D_{xx} = 0.0005$ m²/day, $D_{zz} = 0.0025$ m²/day) correspond to a highly convection-dominated flow. It can be seen that for this case, the solutions show overshoots—small for Courant numbers below unity but large for higher Courant numbers—which may be unacceptable in many cases.

Next, in an attempt to suppress spurious oscillations, the flux limiter for the OCV scheme is used. Fig. 13 shows numerical results for the same case ($P_\Delta = 40$) as previously studied but with the flux limiter in use. The results clearly show that for Courant numbers of unity and below the flux limiter is successful in removing oscillations. But for higher Courant numbers, the flux limiter fails. This by itself is not surprising as the above flux limiter, like most flux limiters, uses only the neighboring cell values to detect oscillations, whereas at high Courant numbers information arrives from far cells. In general, flux limiters have been used for explicit schemes with Courant numbers below unity. No flux limiters used with second-order implicit schemes have yet been demonstrated as effective for high Courant numbers.

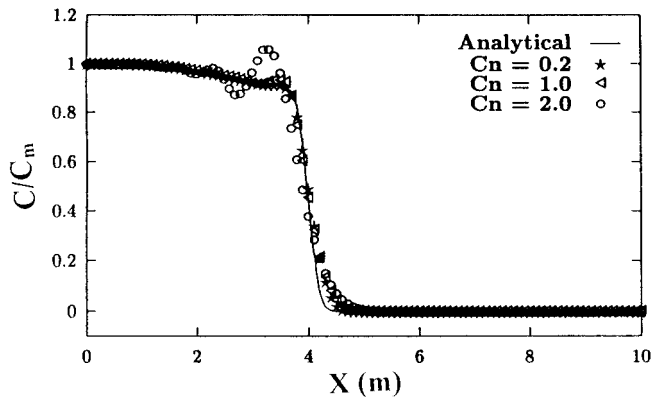A different strategy can be used to avoid overshoots by in-

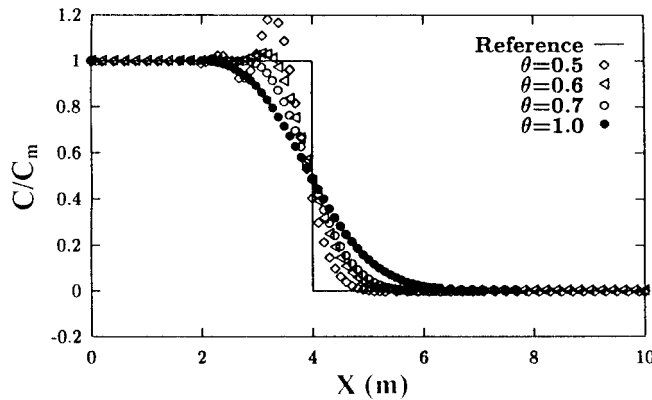**FIG. 13. Longitudinal Concentration Profile Obtained Using Flux Limiter: Test Problem 3 ($P_\Delta = 40$)**

FIG. 14. Effect of θ on Longitudinal Concentration Profile: Test Problem 3 ($P_\Delta = 2000$, $C_n = 2$)
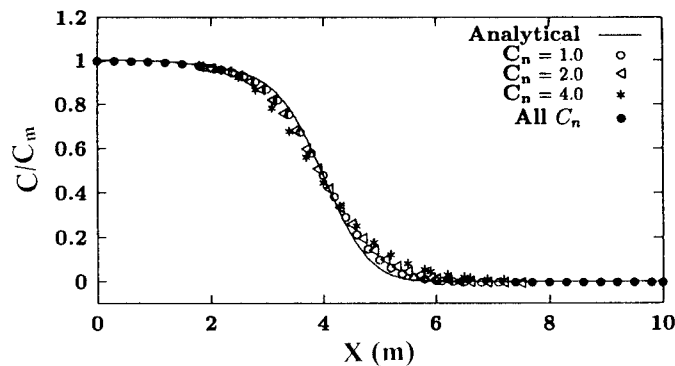

FIG. 15. Longitudinal Concentration Profile: Test Problem 3 ($\theta = 0.7$, $P_\Delta = 2$)
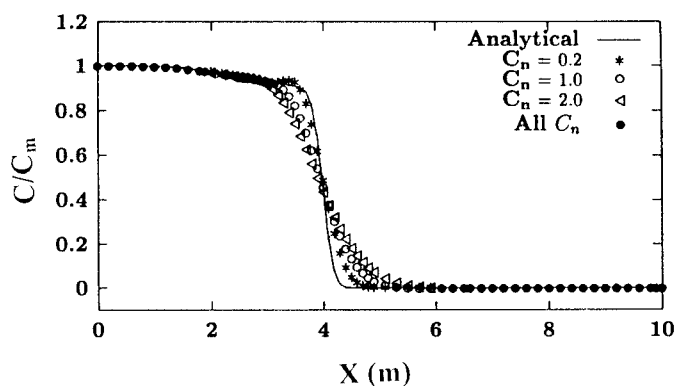

FIG. 16. Longitudinal Concentration Profile: Test Problem 3 ($\theta = 0.7$, $P_\Delta = 40$)

troducing enough numerical dissipation into the scheme by choosing the time-stepping parameter θ as some value other than 0.5. As θ values below 0.5 do not allow unconditional stability, only values above 0.5 are used. To use values other than $\theta = 0.5$ is to introduce a first-order error and numerical diffusion into the time stepping; therefore, it is preferred to make the least departure from that value as possible.

Fig. 14 shows the solutions, for Courant number $C_n = 2.0$ with θ chosen variously, for a very high grid Péclet number of 2,000.0 ($D_{xx} = 0.00001$, $D_{zz} = 0.0$). The figure shows that at $\theta = 0.5$, Crank-Nicholson gives substantial overshoots, which decrease but do not disappear for $\theta = 0.6$. The value $\theta = 0.7$ does not show any overshoots. To increase θ any further would only increase the numerical spreading, as can be seen by the $\theta = 1.0$ solution in the figure. Therefore, for this case at least, $\theta = 0.7$ seems an optimum compromise between numerical dispersion (oscillations) and numerical diffusion (spreading). The scheme performs satisfactorily with $\theta = 0.7$ for a wide range of Courant and grid Péclet numbers.

Figs. 15 and 16 show the same solutions as Figs. 11 and 12, with $P_\Delta = 2$ and 40, respectively, but with solutions time stepped with $\theta = 0.7$ instead of the Crank-Nicholson scheme. The solution shows no overshoots, although slightly more spreading than Crank-Nicholson solutions.

The OCV scheme has been shown to lose little of its accuracy on mildly nonorthogonal grids when applied to steady-state problems (Verma and Eswaran 1996, 1997). Here it is shown that this feature is retained by the present implicitly time-stepped scheme. A new distorted grid is generated by perturbing each interior grid point in Fig. 10 randomly between ±10% of the grid interval in the x-direction. A section of the distorted grid is shown in Fig. 17. Fig. 18 shows the solution at $t = 20$ days on the grids corresponding to Figs. 10 and 17 for $P_\Delta = 2,000$ and $C_n = 1.0$, 2.0, and 4.0. There is
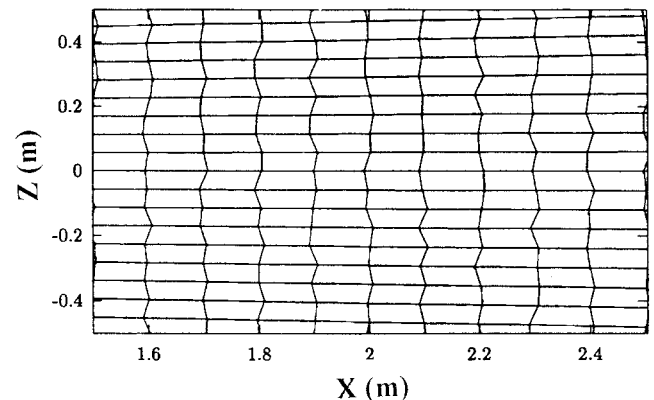

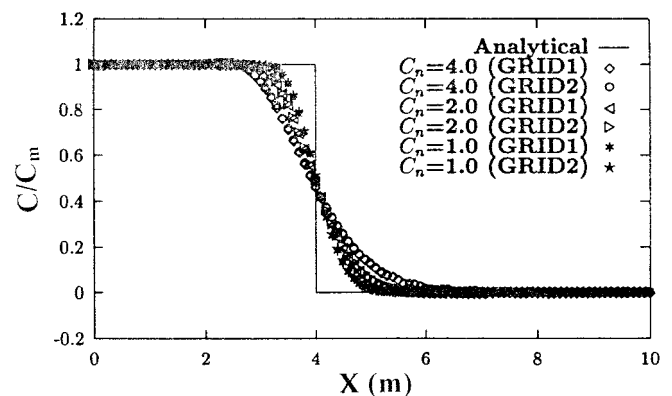**FIG. 17. Distorted Grid for Test Problem 3**

FIG. 18. Effect of Grid Distortion on Longitudinal Concentration Profile: Test Problem 3 ($\theta = 0.7$, $P_\Delta = 2,000$, $C_n > 1$)
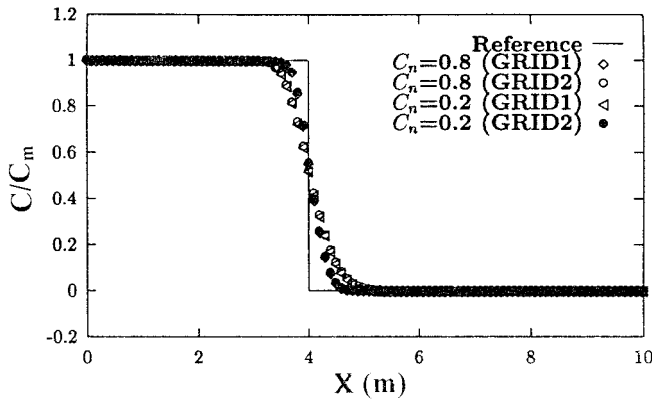
FIG. 19. Effect of Grid Distortion on Longitudinal Concentration Profile: Test Problem 3 ($\theta = 0.7$, $P_\Delta = 2,000$, $C_n < 1$)

little deterioration of accuracy due to grid distortion. This holds true even for C_n below unity, as shown in Fig. 19. These figures also show that numerical spreading of the solution increases unambiguously with the Courant number, as can be expected. The results in Figs. 18 and 19 are obtained using the scheme with $\theta = 0.7$ and the flux limiter. The flux limiter does not seem to affect the final solution for a Courant number greater than unity but does stabilize the time-stepping scheme. For example, in this case without the flux limiter, there could not be convergence beyond $C_n = 1.0$. (However, if convergence is obtained for $C_n > 1$, the solutions with and without the flux limiter are almost the same.)

CONCLUSIONS

In this study, an OCV technique is presented for solving the transient 2D solute transport equation for ground-water flows. Considered are 2D domains with orthogonal and nonorthogonal grids. An isoparametric formulation is used to compute diffusion and to introduce higher order upwinding. An implicit formulation is used for time stepping.

The numerical technique is verified using the 2D analytical solutions. The test cases for verification include Dirichlet, Neumann, and mixed boundary conditions. It is shown that the Crank-Nicholson scheme is most accurate for diffusion-dominated flows (with grid Péclet number <2) but introduces spurious oscillations for convection-dominated flows. The flux limiter used in this study can remove the oscillations for Courant numbers below unity. For higher Courant numbers in convection-dominated flows, spurious oscillations can be avoided by using a value other than 0.5 for the implicit weighting factor; although because of this, the scheme does not retain formal second-order accuracy. For a wide range of Courant and grid Péclet numbers, $\theta = 0.7$ is shown to result in an optimum compromise between numerical dispersion (oscillations) and numerical diffusion (spreading). The effect on accuracy of mild nonorthogonality of the grids is shown to be insignificant.

APPENDIX I. TERMS

Diffusion Terms

For the face 1 (i.e., $k = 1$) at the midpoint (i.e., $\xi = 0$, $\eta = -1$) of the control surface as shown in Figs. 1(b and c), the diffusion coefficients are shown below

$$DIFF\_1(kk) = \left(D_{xx}^{(1)} \frac{\partial N_{kk}}{\partial x} \bigg|_{(0,-1)} \Delta z^{(1)} + D_{xz}^{(1)} \frac{\partial N_{kk}}{\partial z} \bigg|_{(0,-1)} \Delta z^{(1)} \right.$$

$$\left. - D_{zx}^{(1)} \frac{\partial N_{kk}}{\partial x} \bigg|_{(0,-1)} \Delta x^{(1)} - D_{zz}^{(1)} \frac{\partial N_{kk}}{\partial z} \bigg|_{(0,-1)} \Delta x^{(1)} \right)$$

where $kk = 1$–5 are the local node numbers in the counter-clockwise sense, as shown in Fig. 1(c). The other terms on the right-hand side of the above expression have already been defined. Similarly for the control-volume faces 2–4, the diffusion coefficients are, respectively, as follows:

$$DIFF\_2(kk) = \left(D_{xx}^{(2)} \frac{\partial N_{kk}}{\partial x} \bigg|_{(1,0)} \Delta z^{(2)} + D_{xz}^{(2)} \frac{\partial N_{kk}}{\partial z} \bigg|_{(1,0)} \Delta z^{(2)} \right.$$

$$\left. - D_{zx}^{(2)} \frac{\partial N_{kk}}{\partial x} \bigg|_{(1,0)} \Delta x^{(2)} - D_{zz}^{(2)} \frac{\partial N_{kk}}{\partial z} \bigg|_{(1,0)} \Delta x^{(2)} \right)$$

$$DIFF\_3(kk) = \left(D_{xx}^{(3)} \frac{\partial N_{kk}}{\partial x} \bigg|_{(0,1)} \Delta z^{(3)} + D_{xz}^{(3)} \frac{\partial N_{kk}}{\partial z} \bigg|_{(0,1)} \Delta z^{(3)} \right.$$

$$\left. - D_{zx}^{(3)} \frac{\partial N_{kk}}{\partial x} \bigg|_{(0,1)} \Delta x^{(3)} - D_{zz}^{(3)} \frac{\partial N_{kk}}{\partial z} \bigg|_{(0,1)} \Delta x^{(3)} \right)$$

$$DIFF\_4(kk) = \left(D_{xx}^{(4)} \frac{\partial N_{kk}}{\partial x} \bigg|_{(-1,0)} \Delta z^{(4)} + D_{xz}^{(4)} \frac{\partial N_{kk}}{\partial z} \bigg|_{(-1,0)} \Delta z^{(4)} \right.$$

$$\left. - D_{zx}^{(4)} \frac{\partial N_{kk}}{\partial x} \bigg|_{(-1,0)} \Delta x^{(4)} - D_{zz}^{(4)} \frac{\partial N_{kk}}{\partial z} \bigg|_{(-1,0)} \Delta x^{(4)} \right)$$

where $kk = 1$–5. If we define local nodes 1–4 as the west, south, east, and north neighbors, respectively, for the node p, the final expression for the diffusion coefficients for a control volume can be expressed

$$D_W = DIFF\_1(1) + DIFF\_2(1) + DIFF\_3(1) + DIFF\_4(1)$$

$$D_S = DIFF\_1(2) + DIFF\_2(2) + DIFF\_3(2) + DIFF\_4(2)$$

$$D_E = DIFF\_1(3) + DIFF\_2(3) + DIFF\_3(3) + DIFF\_4(3)$$

$$D_N = DIFF\_1(4) + DIFF\_2(4) + DIFF\_3(4) + DIFF\_4(4)$$

$$D_P = DIFF\_1(5) + DIFF\_2(5) + DIFF\_3(5) + DIFF\_4(5)$$

Convection Term

For face 1, again at the midpoint, the convection term is approximated

$$CONV\_1 = (C^{(1)} F^{(1)} |_{mid} = (N_k C_k)^{(1)} F^{(1)} |_{mid}, \quad k = 1\text{–}5$$

Here, midpoint is ($\xi = 0$, $\eta = -1$) for the positive value of $F^{(1)}$ and ($\xi = 0$, $\eta = 1$) for the negative $F^{(1)}$. Combining both the possibilities in a single expression, we get

$$CONV\_1 = \max(F^{(1)}, 0)[C\_1(1)C_{i-1,j} + C\_1(2)C_{i,j-1} + C\_1(3)C_{i+1,j}$$

$$+ C\_1(4)C_{i,j+1} + C\_1(5)C_{i,j}] - \max(-F^{(1)}, 0)[C\_11(1)C_{i-2,j-1}$$

$$+ C\_11(2)C_{i-1,j-2} + C\_11(3)C_{i,j-1} + C\_11(4)C_{i-1,j} + C\_11(5)C_{i-1,j-1}]$$

A similar expression for other surfaces (*CONV*_2, *CONV*_3, and *CONV*_4) of a control volume can be obtained. Rearranging the terms and writing expressions for each node of a control volume, we get

$$C_W = [C\_1(1)\max(F^{(1)}, 0) + C\_2(1)\max(F^{(2)}, 0) + C\_3(1)\max(F^{(3)}, 0)$$

$$+ C\_4(1)\max(F^{(4)}, 0)] - [C\_11(4)\max(-F^{(1)}, 0)$$

$$+ C\_44(2)\max(-F^{(4)}, 0)]$$

$$C_E = [C\_1(3)\max(F^{(1)}, 0) + C\_2(3)\max(F^{(2)}, 0) + C\_3(3)\max(F^{(3)}, 0)$$

$$+ C\_4(3)\max(F^{(4)}, 0)] - [C\_22(4)\max(-F^{(2)}, 0)$$

$$+ C\_33(2)\max(-F^{(3)}, 0)]$$

$$C_N = [C\_1(4)\max(F^{(1)}, 0) + C\_2(4)\max(F^{(2)}, 0) + C\_3(4)\max(F^{(3)}, 0)$$

$$+ C\_4(4)\max(F^{(4)}, 0)] - [C\_33(1)\max(-F^{(3)}, 0)$$

$$+ C\_44(3)\max(-F^{(4)}, 0)]$$

$$C_S = [C\_1(2)\max(F^{(1)}, 0) + C\_2(2)\max(F^{(2)}, 0) + C\_3(2)\max(F^{(3)}, 0)$$
$$+ C\_4(2)\max(F^{(4)}, 0)] - [C\_11(3)\max(-F^{(1)}, 0)$$
$$+ C\_22(1)\max(-F^{(2)}, 0)]$$

$$C_P = [C\_1(5)\max(F^{(1)}, 0) + C\_2(5)\max(F^{(2)}, 0) + C\_3(5)\max(F^{(3)}, 0)$$
$$+ C\_4(5)\max(F^{(4)}, 0)]$$

where the subscripts N, S, E, and W denote the neighboring nodes as defined earlier and the remaining terms of $CONV\_1$, $CONV\_2$, $CONV\_3$, and $CONV\_4$ can be included in the term b of (15). Finally, the coefficients can be represented

$$\alpha_P = \theta[C_p - D_P + \max(C_N, 0) + \max(C_S, 0) + \max(C_E, 0)$$

$$+ \max(C_W, 0)] + \frac{R_d A_s}{\Delta t} + \theta \nu R_d A_s$$

$$\alpha_N = \theta[D_N + \max(-C_N, 0)]$$

$$\alpha_S = \theta[D_S + \max(-C_S, 0)]$$

$$\alpha_E = \theta[D_E + \max(-C_E, 0)]$$

$$\sigma_W = \theta[D_W + \max(-C_W, 0)]$$

$$b = SS + \frac{R_d A_s}{\Delta t} C_{i,j} - \theta[\max(C_N, 0)(C_{i,j+1} - C_{i,j}) + \max(C_S, 0)(C_{i,j-1}$$
$$- C_{i,j}) + \max(C_E, 0)(C_{i+1,j} - C_{i,j}) + \max(C_W, 0)(C_{i-1,j} - C_{i,j})]^n$$
$$+ (1 - \theta)[DIFF + CONV + DEC]^n$$

where SS consists of source terms as well as any other terms that cannot be included in the other coefficients defined above.

APPENDIX II.   REFERENCES

Batu, V. (1989). "A generalized two-dimensional analytical solution for hydrodynamic dispersion in bounded media with the first-type boundary condition at the sources." *Water Resour. Res.*, 25(6), 1125–1132.

Batu, V. (1993). "A generalized two-dimensional analytical solute transport model in bounded media for flux-type finite multiple sources." *Water Resour. Res.*, 29(8), 2881–2892.

Cox, R. A., and Nishikawa, J. (1991). "A new total variation diminishing scheme for the solution of advective-dominant solute transport." *Water Resour. Res.*, 27(10), 2645–2654.

Freeze, R. A., and Cherry, J. A. (1979). *Groundwater*, Prentice-Hall, Englewood Cliffs, N.J.

Heinrich, J. C., Huyakorn, P. S., Zienkiewicz, O. C., and Mitchell, A. R. (1977). "An upwind finite element method for two-dimensional convective transport equation." *Int. J. Numer. Methods in Engrg.*, 11, 131–143.

Hirsch, C. (1991). *Numerical computation of internal and external flows*, Wiley, New York.

Huyakorn, P. S., and Pinder, G. F. (1983). *Computational methods in subsurface flow*, Academic, San Diego.

Ijiri, Y., and Karasaki, K. (1994). "A Lagrangian-Eulerian finite element method with adaptive gridding for advection-dispersion problems." *Computational Methods in Water Resour.*, X, 291–298.

Javendel, I., Doughty, C., and Tsang, C. F. (1984). *Groundwater transport: Handbook of mathematical models*, American Geophysical Union, Washington, D.C., 14–19.

Leonard, B. P. (1979). "Stable and accurate convective modeling procedure based on quadratic upstream interpolation." *Comput. Methods Appl. Mech. Engrg.*, 19, 59–98.

Peyret, R., and Taylor, T. D. (1983). *Computational methods for fluid flow*, Springer, New York.

Pinder, G. F., and Shapiro, A. M. (1979). "A new collocation method for the solution of the convection dominated transport equation." *Water Resour. Res.*, 15(5), 1177–1182.

Putti, M., Yeh, W. W. G., and Mulder, W. A. (1990). "A triangular finite volume approach with high resolution upwind terms for the solution of ground water transport equation." *Water Resour. Res.*, 26(12), 2865–2880.

Sun, N. Z., and Yeh, W. W. G. (1993). "A proposed upstream weight numerical method for simulating pollutant transport in ground water." *Water Resour. Res.*, 19(6), 1489–1500.

Van Genuchten, M. Th. (1977). "On the accuracy and efficiency of several numerical schemes for solving the convective-dispersive equation." *Finite element in water resources*, W. G. Gray, G. F. Pinder, and I. A. Brebbia, eds.

Verma, A. K., and Eswaran, V. (1996). "Overlapping control volume approach for convection-diffusion problems." *Int. J. Numer. Methods in Fluids*, 23, 865–882.

Verma, A. K., and Eswaran, V. (1997). "A bounded convection scheme for the overlapping control volume approach." *Int. J. Numer Method in Fluids*, 25, 1137–1161.

Wang, C., Sun, N., and Yeh, W. W. G. (1986). "An upstream weight multiple cell balance finite-element method for solving three-dimensional convection-dispersion equations." *Water Resour. Res.*, 22(11), 1575–1589.

Westerink, J. J., and Shea, D. (1986). "Consistent higher degree Petrov-Galerkin methods for the solution of transient convection-diffusion equation." *Int. J. Numer. Methods in Engrg.*, 28, 1077–1100.

Yeh, G. T. (1986). "An orthogonal upstream finite-element approach to modeling aquifer contaminant transport." *Water Resour. Res.*, 22(6), 952–964.

Yeh, G. T. (1990). "A Lagrangian-Eulerian method with zoomable hidden fine-mesh approach for solving advection-dispersion equations." *Water Resour. Res.*, 26(6), 1133–1144.

Yeh, G. T., and Chang, J. R. (1992). "An exact peak capturing and oscillation-free scheme to solve advection-dispersion transport equations." *Water Resour. Res.*, 28(11), 2937–2951.

Yu, F. X., and Singh, V. P. (1995). "Improved finite-element method for solute transport." *J. Hydr. Engrg.*, ASCE, 121(2), 145–158.

APPENDIX III.   NOTATION

The following symbols are used in this paper:

A_s = area of control volume;
C = solute concentration;
C_n = courant number;
D_h = hydrodynamic dispersion tensor;
D_{xx}, D_{zx}, D_{zz} = elements of dispersion tensor;
dA = elemental area of control volume;
dl = elemental length on control surface;
F = flux across edge of control surface;
(i, j) = node number for control volume;
(k) = superscript for local edge numbers of control volume;
m = subscript for local node numbers of control volume;
$N_1, \ldots, N_5$ = finite-element type shape functions;
n = superscript to denote time level;
n_x, n_z = direction cosines of local outward unit vector on control surface;
P_Δ = grid Péclet number;
R_d = retardation factor;
t = time;
u = velocity in x-direction;
$\mathbf{V}$ = pore-water velocity vector;
w = velocity in z-direction;
x = x-coordinate;
z = z-coordinate;
Δt = computational time step;
Δx = change in x-coordinate along edge of control surface;
Δz = change in z-coordinate along edge of control surface;
η = local coordinate for transformed element corresponding to z;
θ = implicit weighting parameter;
λ = first-order decay coefficient;
ξ = local coordinate for transformed element corresponding to x; and
ϕ = porosity.